Trajectory-Tracking of UHF RFID Tags, Exploiting Phase Measurements Collected from Fixed Antennas

Aristidis Raptopoulos Chatzistefanou, Anastasios Tzitzis, Spyros Megalou, George Sergiadis, *Member, IEEE,* Antonis G. Dimitriou, *Senior, IEEE*

***Abstract*—In this paper we propose a novel method for tracking a moving UHF RFID tag in 3D space. The tag moves in an area monitored by at least two antennas fixed at known locations. Phase measurements from each antenna are collected. Assuming a grid of N initial positions, we calculate N possible trajectories, by deriving closed form expressions, exploiting only the phase measurements collected by each antenna separately. Then, using the measured phase-difference from each antenna-pair, a hyperbola's branch on which the tag must be located is calculated. We evaluate the distance of each trajectory from the hyperbolas. Finally, we select the trajectory that minimizes the distance. Experimental results, conducted with a SLAM (Simultaneous Localization and Mapping)-enabled robot show a mean error less than 20cm with estimations derived in the order of ms. Compared to prior art, the proposed method does not assume neither knowledge of the trace, nor of the initial position of the tag. Furthermore, it accomplishes high accuracy at reduced computation time.**

***Index Terms*—phase, RFID, tracking, trajectory.**

I. Introduction

Radio Frequency Identification (RFID) technology experiences widespread penetration in the logistics, health care, and security market. Tracking of moving RFID tagged items/people is expected to empower new applications, e.g. personnel tracking, luggage tracking, travellers' tracking, to enhance security and reduce delays, etc. Other RFID applications are presented in [1] and [2]. In this paper, we focus on the problem of tracking moving RFID tags by stationary RFID equipment.

In our case, the goal of the method is to track the visitors of the Archaeological Museum of Thessaloniki. The visitors are given their UHF RFID tagged ticket upon entering the museum. Phase and power measurements are collected from commercial RFID readers, installed throughout the museum. Using the tracking data, an enhanced and personalized guided experience is offered to the visitors. Additionally, statistics such as common visiting patterns or the popularity of each exhibit can be extracted.

Prior art on this problem includes approaches varying greatly on the means used, as well as the goal of the tracking. Gesture recognition and the approximation of the shape of the trajectory is examined in [3], [4], and [5], using mainly the measured phase of arrival (POA). In [3] and [4] the monitored area is surrounded by antennas, which is not possible in many applications. In [5], only the shape recognition is evaluated.

Regarding the tracking of moving RFID tags, authors in [6] and [7] place more than one tag (*tag array*) on the target, to reduce the number of required monitoring antennas. In [6] radial velocity vectors are used to calculate the trajectory of a target whose initial position is known; such information is not typically available in tracking applications. In [7], the authors move a single reader's antenna to create a synthetic aperture, instead of installing multiple antennas at fixed locations.

In [8], Received Signal Strength Indicator (RSSI) measurements are used from distributed readers to calculate the trajectory of people with RFID tags in a science museum. RSSI measurements are highly ambiguous due to fading, and yield less accurate tracking results. RSSI-based methods mainly depend on estimating the distance between multiple antennas and the target, e.g. as shown in [9], and locating the target through triangulation. Authors in [10] and [11] surround the target tag with multiple antennas. In [10], they transmit on different operating frequencies to get POA data for different wavelengths and track the tag, using a complex measurement system. Transmission over different carriers is not a good option in Europe, where a very narrow operational bandwidth is allocated, spanning over only 2 MHz. Due to the limited bandwidth, the difference of the wavelengths along different carriers is small and causes a very small difference in the measured backscattered phase. This is typically smaller than the standard deviation of the phase-noise of the reader. In [11] the authors use a Kalman filter and POA measurements to calculate the trajectory. However, the method "needs" the initial position, which is approximated by the collected RSSI measurements; RSSI may lead to large errors, depending on blockage and the effects of multipath. In [12] and [13], the authors track a tag moving on a known trace (e.g. a conveyor belt) using the angle of arrival (AOA) and an inverse synthetic-aperture radar (SAR) approach. In [14], the 3D position and orientation of a tag is calculated, provided that a specific 3-antenna set-up is followed. Similarly to [6] and [11], the method in [14] is also constrained on knowledge of the initial position of the target. Authors in [15] develop a method for tracking utilizing POA measurements from multiple antennas at known locations, for a target moving on a known trajectory.

Manuscript received January 5, 2021
This research has been co-financed by the European Union and Greek national funds through the Operational Program Competitiveness, Entrepreneurship and Innovation, under the call RESEARCH – CREATE – INNOVATE (project code:T2EDK-02000).

All authors are with the School of Electrical and Computer Engineering, Aristotle University of Thessaloniki, Greece, e-mail: antodimi@auth.gr.

However, when the method is applied for an arbitrary trajectory, it's time complexity increases. Consequently, the method is unsuitable for real-time tracking of targets at arbitrary trajectories.

Other works focus on *device-free* tracking; that is, tracking a moving target that is not carrying a RF device. The authors in [16], [17] and [18], leverage the multipath effect to track targets that do not carry RFID tags, using measurements from tags in the monitored area; they monitor changes in the measured pattern from the fixed RFID-tags. An excessive training phase in [16] and [18], and a complex RFID system installation is required. A similar installation is used in [19] and [20], in which a target moving in an area covered by a wireless sensor network (WSN) grid is tracked. A major disadvantage of these methods is that the tracked target cannot be identified.

Tracking is also achieved using the widespread 802.11 network. RADAR is introduced in [21]. During an *offline phase*, a node collects RSSI information from various base stations at different positions of the monitored area. Then, in the *online phase*, measurements are compared to the collected data to track the moving node. Authors in [22] also use RSSI information, and additionally leverage channel state information (CSI) to counter the multipath effect. A time of arrival (TOA) based method is developed in [23], to calculate the distance of the target from base stations, and by triangulation track the target. A device-free approach is examined in [24]. Deep neural networks (DNN) and particle filters (PF) are used to track moving targets by the changing CSI. However, the tracking error in these methods is in the order of meters.

Non-RF methods include works like [25], [26], and [27]. Tracking in [25] is achieved leveraging data from smartphone sensors, requiring special software on the mobile terminals. A 360^o lidar is used in [26], meaning that the identity of the target is unknown. Multiple cameras, after a training phase, are used in [27]. An overview of the mentioned methods is shown in Table I.

In this paper, we propose a novel method for RFID trajectory tracking using POA measurements of the target tag, collected from multiple antennas at known locations, using only commercial RFID equipment. Given that our goal is to track visitors inside an exhibition area, the following requirements must be met:

- There is no information on the initial location of the targets. Visitors may enter the "tracking zone" from any location.
- The targets are expected to perform any arbitrary movement, including stops.
- The speed is expected to be smaller than the typical human walking speed of 1.4m/s. Given a read-rate of 300 tags/s and the small density of visitors per m^2, each target-tag is expected to be identified multiple times per s (and therefore per m).
- The computational requirements must be such, that the trajectory is estimated in real-time.
- Tracking should be accurate enough to allow discrimination of one's visiting-zone per exhibit and per unit of time; i.e. we should be able to determine how much time each visitor spent on each exhibit. Depending on the exhibition's configuration, the accuracy should be better than 1m.
- Commercial UHF RFID tags will be deployed. Considering this, we deploy commercial RFID readers.

The proposed method exploits the unwrapped phase measurements collected by multiple antennas. Possible trajectories are initially calculated, through closed-form expressions, given the set of measurements collected from **each** antenna. Then the best trajectory is selected by exploiting the phase-difference of the measurements from each **pair** of antennas, again by closed-form equations.

In section II, the proposed method is described. Implementation of the method is given in section III. Simulation results are presented in section IV. In section V, we conduct experiments, deploying a SLAM capable terrestrial robot, in order to compare with the ground-truth trajectory of the tag, extracted from the robot. A comparison with prior art is given in section VI. Limitations and future work is discussed in section VII. Finally, our conclusions are presented in section VIII.

II. Proposed Tracking Method

The proposed method tracks a moving RFID tag. The tag is interrogated by multiple antennas of an RFID reader. All antennas are at known locations. Phase measurements of the received signal from each antenna are collected. The method can be decomposed in the following Steps:

1) The collected phase measurements are unwrapped and filtered.
2) We consider N_P possible initial tag positions in the monitored area.
3) For each initial position, we estimate the subsequent locations of the tag, given the collected phase measurements from each antenna. This results to N_P possible trajectories.
4) Selection of the best (among N_P) trajectory is performed by calculating the sum of distances of all points of each trajectory from the *hyperbolas* that correspond to the *measured* phase-differences of the tag's backscattered signal at different antennas.

A. Step 1: Phase Unwrapping and Filtering

The measured phase of the tag's backscattered signal is wrapped in $[0, 2\pi)$. Thanks to the reader's read-rate, typically exceeding 200 reads/s, the wrapping points can be recognized. and the phase measurement is easily unwrapped. Additionally, real measurements always include noise, which is modeled as a normally distributed variable. So, the measured phase is:

$$\phi_{meas} = (\phi + \phi_{noise}) \, mod \, (2\pi) \tag{1}$$

$$\phi = \phi_p + \phi_o \tag{2}$$

$$\phi_p = \frac{4\pi}{\lambda} d \tag{3}$$

TABLE I
TRACKING METHODS OVERVIEW.

Ref.	Technology	Measured Quantity	No. of Antennas	Reported Accuracy (cm)	Needs Initial Position	Method	Comments
[3]	RFID	POA, RSSI	≥ 4	23.4	Yes	Direction	Initial Position by RSSI
[4]	RFID	POA	≥ 4	31.8	No	Direction	-
[5]	RFID	POA	1	-	No	Direction	No accuracy evaluation.
[6]	RFID	POA	1	3.2 (y-error)	Yes	Other	1D accuracy.
[7]	RFID	POA, RSSI	1	13.6	Yes	Other	Uses spinning antenna.
[8]	RFID	RSSI	≥ 2	280	No	Probabilistic	-
[10]	RFID	POA	≥ 2	3.6	No	Geometrical	Multiple carrier frequencies.
[11]	RFID	POA, RSSI	≥ 4	1.5 (anechoic)	Yes	Kalman Filter	Initial Position by RSSI.
[12]	RFID	POA	≥ 4	-	No	Direction	Known trajectory.
[13]	RFID	POA	1	5.1	No	Other	Known trajectory.
[14]	RFID	POA, RSSI	3	4.3	Yes	Other	-
[15]	RFID	POA	≥ 2	12.3 (median)	No	Other	-
[16]	RFID	POA	2	1.4	No	Other	Cannot identify target.
[17]	RFID	POA	-	54.3	No	Other	Cannot identify target.
[18]	RFID	POA	1	9.8 (median)	No	Other	Cannot identify target.
[19]	WSN	RSSI	-	100	No	Other	Cannot identify target.
[20]	WSN	RSSI	-	94	No	Other	Cannot identify target.
[21]	802.11	RSSI	-	350	No	Triangulation	-
[22]	802.11	RSSI	-	120	No	Triangulation	-
[23]	802.11	TOA	-	-	No	Triangulation	Wideband system.
[24]	802.11	RSSI	-	54	No	Other	Cannot identify target.
[25]	Smartphone sensors	Other	-	49	Yes	Probabilistic	-
[26]	360^o Lidar	-	-	2	No	Other	Cannot identify target.
[27]	Cameras	-	-	13	Yes	Other	Cannot identify target.
This Work	RFID	POA	≥ 2	20	No	Other	Realtime and 3D.

$$\phi_{noise} : N \sim (0, s_{phase}) \tag{4}$$

ϕ is the phase of the received signal, ϕ_p is the phase accumulated due to the electromagnetic wave propagation, ϕ_o is a phase offset including phases of the cables and the related hardware, ϕ_{noise} is the phase measurement noise, λ is the wavelength of the electromagnetic field, and d is the distance from the antenna to the tag.

An example of wrapped and unwrapped phase measurements is shown in Fig. 1.

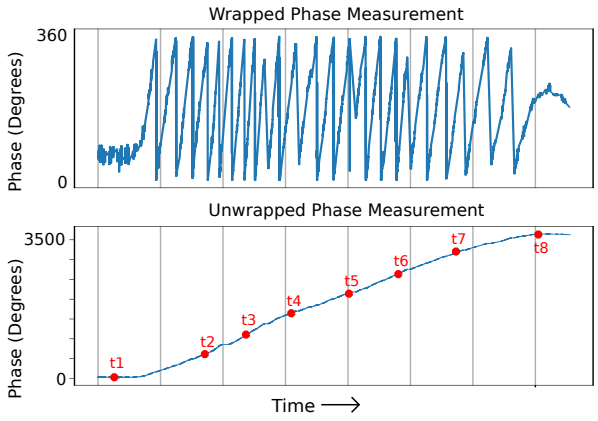

Fig. 1. The top plot shows phase measurements wrapped in $[0, 360)$. The bottom plot shows the same measurements, unwrapped. Times $t_1, t_2, \ldots, t_8$ form the time set at which the trajectory of the tag will be calculated. The unwrapped phase difference between subsequent times of the time-set is much greater than the phase measurement noise.

After unwrapping, a second-degree Savitzky–Golay filter is applied to the data. As a result, the signal is smoothed and the error between the measurements and the "real" phase values is reduced. An example of the above is shown in Fig. 2. Simulation results show the error between the noiseless and noisy data is reduced by $\sim 75\%$ when the filter is applied.

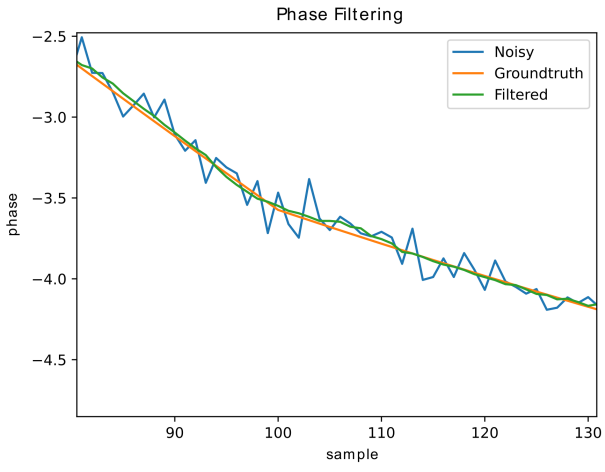

Fig. 2. An example of phase filtering as described in section II-A. The yellow line represents the real phase values, without noise. The blue line is the noisy measurement. The green line is the result of the filter being applied to the blue line.

B. Step 3: Trajectory Calculation

Here, the trajectory calculation of Step 3 from section II is described. Assuming the initial position of the tag, its positions at following times can be calculated using phase measurements from each antenna.

Let A_i be the position of Antenna-i in three-dimensional space. Antenna-i lies on the $z = H_i$ plain. At time t the tag's position is T_t. The tag lies on the $z = h_t$ plain. $P_{i,t}$ is the projection of A_i on the $z = h_t$ plain. Let $dh_{i,t}$ be the height difference between Antenna-i and the tag:

$$dh_{i,t} = H_i - h_t \tag{5}$$

If $R_{i,t}$ is the distance between A_i and T_t, and $r_{i,t}$ is the distance between $P_{i,t}$ and T_t, the expected phase measurements should be:

$$R_{i,t}^2 = (dh_{i,t})^2 + (r_{i,t})^2 \tag{6}$$

An illustration of the above is shown in Fig. 3. Let the phase received by Antenna-i at time t be $\phi_{i,t}$. According to (2) and (3):

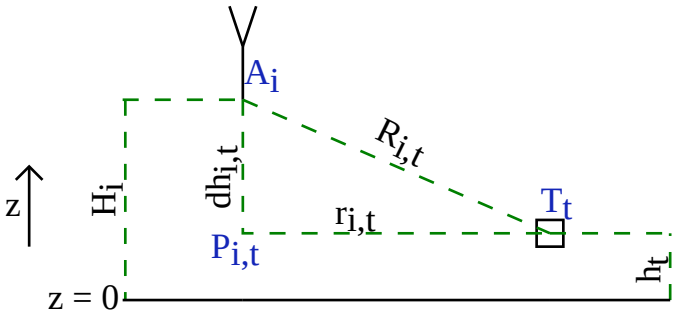

Fig. 3. A_i is the position of Antenna-i. T_t is the position of the tag at time t. $P_{i,t}$ is the projection of A_i on the $z = h_t$ plain. $H_i, h_i, dh_{i,t}, R_{i,t}$ and $r_{i,t}$ are various distances regarding Antenna-i and the tag.

$$\phi_{i,t} = \frac{4\pi}{\lambda} R_{i,t} + \phi_o \tag{7}$$

Let $d\phi^i_{t1,t2}$ denote the difference of expected phases measured at the same antenna i at time instances t_1, t_2:

$$d\phi^i_{t1,t2} = \phi_{i,t2} - \phi_{i,t1} \tag{8}$$

Equation (8) allows us to remove the common unknown value of ϕ_0. Substituting (7) in (8):

$$\begin{aligned} d\phi^i_{t1,t2} &= \frac{4\pi}{\lambda} R_{i,t2} + \phi_o - \frac{4\pi}{\lambda} R_{i,t1} - \phi_o \\ d\phi^i_{t1,t2} &= \frac{4\pi}{\lambda} (R_{i,t2} - R_{i,t1}) \\ R_{i,t2} &= R_{i,t1} + \frac{d\phi^i_{t1,t2}}{g} \end{aligned} \tag{9}$$

where $g = \frac{4\pi}{\lambda}$. Substituting (6) in (9):

$$\begin{aligned} \sqrt{(r_{i,t2})^2 + (dh_{i,t2})^2} &= R_{i,t1} + \frac{d\phi^i_{t1,t2}}{g} \\ r_{i,t2} &= \sqrt{\left| \left(R_{i,t1} + \frac{d\phi^i_{t1,t2}}{g} \right)^2 - (dh_{i,t2})^2 \right|} \end{aligned} \tag{10}$$

According to (10) T_{t2}, is in a circle on the $z = h_{t2}$ plain, with center $P_{i,t2}$ and radius $r_{i,t2}$. Let that circle be $C_{i,t2}$. So far, from two unwrapped phase measurements, collected by the same antenna, we can calculate the circle where the tag should be located, **given that its position at the initial time instant is known**. It is noted that the proposed method does not require knowledge of the initial position of the target, but leverages the analysis of this section by assuming it.

By repeating this process for two additional reader-antennas - for the same *known* initial point - we can calculate the tag's position from the intersection of the three resulting circles, as explained next. Let's assume that a tag in a **known** position is interrogated by (at least) three antennas, Antenna-1, Antenna-2 and Antenna-3, at times $t = t1$ and $t = t2$. Using phase measurements from each antenna, $d\phi^i_{t1,t2} : i = 1, 2, 3$ can be calculated. If g, T_{t1}, A_1, A_2, A_3 and h_{t2} are also known, $r_{i,t2} : i = 1, 2, 3$ can be calculated using (10). Additionally, since A_1, A_2, A_3 and h_{t2} are known, the antennas' projections $P_{1,t2}, P_{2,t2}, P_{3,t2}$ on the $z = h_{t2}$ plain are known as well. Therefore, the centers and radii of the circles $C_{i,t2}$ for $i = 1, 2, 3$ can be calculated. The position of the tag T_{t2} at time $t = t2$ is the intersection of these three circles. The above is illustrated in Fig. 4.

By deploying this method, the trajectory of the tag can be calculated assuming any starting position in the search area and the set of phase-measurements collected by the reader's antennas. It should be noted that due to the ground-plane of typical microstrip reader-antennas, the read-range of each antenna is limited in the space in front of the antenna. As a consequence, the trajectory can be calculated using only two antennas, assuming that they are both placed on the same plane, e.g. on the same wall. The second intersection of the two circles would appear within the area located at the back of the antennas.

C. Step 4: Trajectory Evaluation

Thanks to the process described previously, for any initial position, one can calculate a "valid" trajectory according to the phase measurements. Assuming N_p initial positions, one will end up with N_p trajectories. We will show next how to select the best trajectory.

The phase difference between antennas is used to calculate the hyperbola's branch on which the tag lays. Then, the distance between each trajectory's positions and the corresponding branches is calculated. Based on this, a weight is applied to each trajectory, as explained in section III-F. The trajectory closest to the corresponding branches is selected as the estimated trajectory of the tag. Below, the branch creation and the distance calculations are explained in detail.

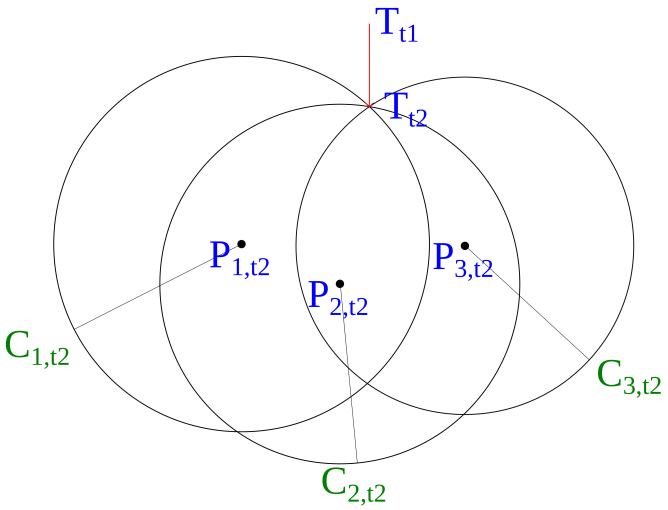

Fig. 4. $P_{1,t2}, P_{2,t2}, P_{3,t2}$ are the antennas' projections on the $z = h_{t2}$ plain at time $t = t2$. T_{t1}, T_{t2} are the positions of the tag at times $t = t1$ and $t = t2$. The red arrow represents how the tag moves. $C_{i,t2}$ is the circle on which lies T_{t2}, based on phase measurements from Antenna-i, if T_{t1} and the z-coordinate of T_{t2} is known. The intersection of three such circles is T_{t2}.

1) Hyperbola's branch: The tag at position T_t is interrogated by two antennas at positions A_1 and A_2. Let $d\phi_t^{1,2}$ be the difference of the phase measurements of the two antennas at time t:

$$d\phi_t^{1,2} = \phi_{2,t} - \phi_{1,t} \tag{11}$$

Substituting (7) in (11):

$$d\phi_t^{1,2} = g(R_{2,t} - R_{1,t}) \tag{12}$$

We want to find the possible positions of the tag which would result in the same $d\phi_t^{1,2}$ measurements. If $H_1 = H_2 = H$ and h_t is known, then:

$$dh_{1,t} = dh_{2,t} = dh_t = H - h_t \tag{13}$$

Equation (13) shows that points $P_{1,t}, P_{2,t}$ are on the $z = h_t$ plain. Let $P_{1,t}, P_{2,t}$ be on the $x\ axis$ so that $P_{1,t}(x_0, 0)$ and $P_{2,t}(-x_0, 0)$ We assume that the tag can only be on the $z = h_t$ plain. $\tilde{T}(x, y)$ is a possible position. Equation (12) can be written as:

$$\begin{aligned} \frac{d\phi_t^{1,2}}{g} &= \sqrt{(P_{2,t}\tilde{T})^2 + dh_t^2} - \sqrt{(P_{1,t}\tilde{T})^2 + dh_t^2} \\ \frac{d\phi_t^{1,2}}{g} &= \sqrt{(x + x_0)^2 + y^2 + dh_t^2} \\ &\quad - \sqrt{(x - x_0)^2 + y^2 + dh_t^2} \\ \Rightarrow\ & a_1 x^2 + a_2 y^2 + a_3 = 0 \end{aligned} \tag{14}$$

Where:

$$a_1 = \left(\frac{d\phi_t^{1,2}}{g}\right)^2 - 4x_0^2 \tag{15}$$

$$a_2 = \left(\frac{d\phi_t^{1,2}}{g}\right)^2 \tag{16}$$

$$a_3 = \left(\frac{d\phi_t^{1,2}}{g}\right)^2 \left(x_0^2 + dh_t^2 - 0.25\left(\frac{d\phi_t^{1,2}}{g}\right)^2\right) \tag{17}$$

The maximum value of $d\phi_t^{1,2}$ is measured, if the tag is on the line that connects A_1 and A_2. Since A_1 and A_2 have the same z-coordinate, their distance is the same as $P_{1,t}$ and $P_{2,t}$:

$$\begin{aligned} \left|d\phi_t^{1,2}\right| &\le g(P'_{1,t}P'_{2,t}) = 2g\,|x_0| \\ \Longrightarrow \left(\frac{d\phi_t^{1,2}}{g}\right)^2 &\le 4x_0^2 \end{aligned} \tag{18}$$

Using (18) the signs of a_1, a_2, a_3 can be calculated:

$$\begin{aligned} a_1 &= \left(\frac{d\phi_t^{1,2}}{g}\right)^2 - 4x_0^2 \\ &\Rightarrow a_1 \le 0 \end{aligned} \tag{19}$$

$$\begin{aligned} a_2 &= \left(\frac{d\phi_t^{1,2}}{g}\right)^2 \\ &\Rightarrow a_2 \ge 0 \end{aligned} \tag{20}$$

$$\begin{aligned} a_3 &= \left(\frac{d\phi_t^{1,2}}{g}\right)^2 \left(x_0^2 + dh_t^2 - 0.25\left(\frac{d\phi_t^{1,2}}{g}\right)^2\right) \\ a_3 &= \left(\frac{d\phi_t^{1,2}}{g}\right)^2 \left(0.25\left(4x_0^2 - \left(\frac{d\phi_t^{1,2}}{g}\right)^2\right) + dh_t^2\right) \\ &\Rightarrow a_3 \ge 0 \end{aligned} \tag{21}$$

Expressions (19), (20), (21) show that (14) is the equation of a hyperbola whose center is $O(0, 0)$, and major axis the $x\ axis$. The two branches of the hyperbola are:

$$x = \pm\sqrt{-\frac{a_2}{a_1}y^2 - \frac{a_3}{a_1}} \tag{22}$$

Knowing $d\phi_t^{1,2}$ limits the possible tag positions to one branch only. If $d\phi_t^{1,2} > 0$, (12) shows that T_t is closer to A_1, and subsequently to $P_{1,t}$. Similarly, if $d\phi_t^{1,2} < 0$, T_t is closer to $P_{2,t}$. This can be expressed as:

$$s_{ign} = sign(x_0 d\phi_t^{1,2}) \tag{23}$$

$$x = s_{ign}\sqrt{-\frac{a_2}{a_1}y^2 - \frac{a_3}{a_1}} \tag{24}$$

It is reminded that in (13) we assumed that the two antennas are at the same height. If there is a height difference between them, the locus matching the measured phase difference is either a hyperbola, as shown above, or an ellipse. However, regarding practical antenna positions, measurement points resulting to an elliptic locus are beyond the antennas' "visible" area. The proposed method can also be applied in such cases.

2) Distance from hyperbola's branch: Next, we want to calculate the distance between a point to a hyperbola's branch. This will be used for the selection of the actual trajectory of the tag; the smallest distance corresponds to the most valid estimation.

In section II-C1, the branches' equation was calculated for antenna-positions on the $x\ axis$. However, the position of the antennas can be arbitrary. In that case, a different coordinate system is used to transform the antennas as those of section II-C1.

Let $A(x_a, y_a), B(x_b, y_b), M(x_m, y_m)$ be three points and their coordinates on the original coordinate system. We want to transform them to $A'(x_0, 0), B'(-x_0, 0), M'(x'_m, y'_m)$. This can be achieved by a simple rotation and displacement of the coordinate system. We will represent this transform as:

$$F\left(A, B, M\right) = [x_0, M'(x'_m, y'_m)] \tag{25}$$

An illustration of the transform is shown in Fig. 5. The new coordinates are calculated as following:

$$\begin{aligned} x_0 &= cos(\theta)\frac{(x_a - x_b)^2 + (y_a - y_b)^2}{2(x_a - x_b)} \\ x'_m &= cos(\theta)(x_m + dx) + sin(\theta)(y_m + dy) \\ y'_m &= -sin(\theta)(x_m + dx) + cos(\theta)(y_m + dy) \\ dx &= -\frac{x_a + x_b}{2} \\ dy &= -\frac{y_a + y_b}{2} \\ \theta &= arctan\left(\frac{y_a - y_b}{x_a - x_b}\right) \end{aligned} \tag{26}$$

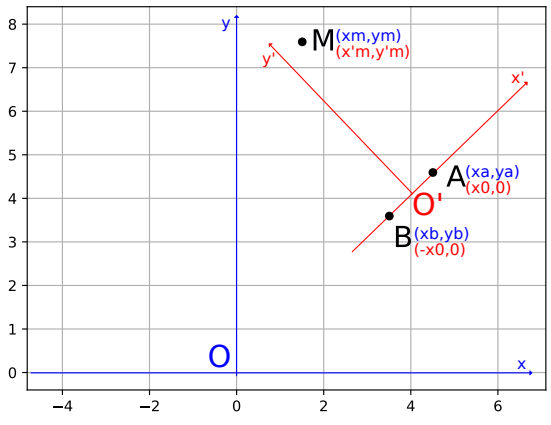

Fig. 5. An illustration of $F\left(A, B, M\right)$ transform. The blue notation represent the original coordinate system, and the red the new one. The line that connects A and B is the $x'\ axis$ of the new coordinate system. Its center O' is the center of the AB line segment.

So, to calculate the distance from point $\tilde{T}$ of the "global" coordinate system to the hyperbola's branch, expressed in a "local" coordinate system for arbitrary antenna positions $P_{1,t}, P_{2,t}$, the transform of (25) is applied:

$$F\left(P_{1,t}, P_{2,t}, \tilde{T}\right) = [x_0, \tilde{T}'(x_t, y_t)] \tag{27}$$

x_0 is used to calculate the branch equation of (24). The distance D_{HP} from a point (x', y') of the branch to $\tilde{T}'$ is:

$$D_{HP}(x', y') = \sqrt{\left(x' - x_t\right)^2 + \left(y' - y_t\right)^2} \tag{28}$$

By substituting (24) in (28) we get:

$$D_{HP}(y') = \sqrt{\left(s_{ign}\sqrt{-\frac{a_2}{a_1}y'^2 - \frac{a_3}{a_1}} - x_t\right)^2 + \left(y' - y_t\right)^2} \tag{29}$$

The minimum value of (29) is d_{is}. Differently, d_{is} is the square root of the minimum value of D^2_{HP}. D^2_{HP} is minimum when:

$$\begin{aligned} &\frac{\partial D^2_{HP}}{\partial y'} = 0 \\ &\left(1 - \frac{a_2}{a_1}\right)y' - y_t + \frac{s_{ign}x_t\frac{a_2}{a_1}y'}{\sqrt{-\frac{a_2}{a_1}y'^2 - \frac{a_3}{a_1}}} = 0 \\ &\frac{\left(x_t\frac{a_2}{a_1}\right)^2 y'^2}{-\frac{a_2}{a_1}y'^2 - \frac{a_3}{a_1}} = \left[\left(1 - \frac{a_2}{a_1}\right)y' - y_t\right]^2 \end{aligned} \tag{30}$$

Equation (30) is a forth-degree polynomial equation. By calculating its roots and substituting them to (29), d_{is} is found.

III. Implementation

In this section, we describe how the proposed method was implemented for simulations and experiments.

A. Step 2: Generation of Initial Positions

N_P initial positions are randomly generated within the area in which the tag may be identified. The area is bounded by the reader's maximum range and the building's boundaries.

B. Step 3: Time-set Creation

It is not required to calculate the position of the tag when it does not move. Additionally, if the tag is carried by a human, its trajectory will consist of almost linear segments. Such segments are decently represented by very few of their points. So, the trajectory of the tag is calculated at longer time intervals than those of the collected measurements, but still greatly represents the real trajectory. Additionally, the computational requirements are reduced and bad phase measurements can be avoided.

Let $TimeSet\left([t_1, t_2, \ldots, t_{Nt}]\right)$ be the times at which the trajectory is calculated. These are chosen in such a way that the phase differences used in calculation are much greater than the expected variability of the measurements' zero-mean Gaussian noise.

The starting time t_1 is the time the measurements begin. Then the cumulative absolute phase variation is calculated for the filtered phase measurements of each antenna. If $pAfil(t)$ are the filtered phase measurements from antenna A, then the absolute phase variation for antenna A is $cA(t)$:

$$cA(t) = \begin{cases} 0, t \leq t_1 \\ |pAfil(t) - pAfil(t_1)|, t > t_1 \end{cases} \quad (31)$$

Equation (31) will be used as a metric of how much the measured phase varies vs. time, and, consequently, how much the tag moves. The measured phase depends on the distance between the antenna and the tag. If the tag is still, the measured phase does not change. If the tag moves, its distance from the antenna changes and so does the measured phase.

One needs to assess whether the tag's movement was significant. The tag is monitored by N_{ant} antennas $A_1, A_2, \ldots, A_{N_{ant}}$. Let t_1 denote the most recent time-instance added to the time-set. We wish to select time $t_2 > t_1$ which will be the next time-instance added to the time-set. The value of t_2 is initialized at t_1 ($t_2 := t_1$), and then is increased by small time steps ($t_2 := t_2 + timeStep$), until the following condition is met:

$$\frac{\sum_{i=1}^{N_{ant}} (cA_i(t_2) - cA_i(t_1))}{N_{ant}} \geq phThr \quad (32)$$

Equation (32) is the mean of the change of the measurements from all antennas. This value is compared with a phase variation threshold $phThr$. The value of this threshold is chosen to be much greater than the measurement noise standard deviation. Measurements show that the standard deviation is approximately 0.1 radians. So, suitable values for $phThr$ are $2\pi, 3\pi$, etc., which correspond to displacement of the tag in the order of $0.17m, 0.26m$, etc.

The remaining times $t_3, t_4, \ldots, t_{Nt}$ are calculated in the same manner. An example of a time-set is shown in Fig. 1.

C. Step 3: Possible Trajectories Calculation

At the start t_1 of the time-set, N_P possible positions of the tag are randomly generated. These positions Pos_1^j, $j = 1, 2, \ldots, N_P$ represent the possible positions of the tag at t_1. Since the position of the tag is assumed at t_1, the process described in section II-B can be used to determine its position at the remaining times of $TimeSet\,([t_1, t_2, \ldots, t_{Nt}])$.

Starting from the known position at t_1 and applying the process of section II-B on pairs of subsequent times in $TimeSet$, positions at all the times of $[t_1, t_2, \ldots, t_{Nt}]$ can be calculated. The times $[t_1, t_2, \ldots, t_{Nt}]$ and the corresponding positions $\left[Pos_1^j, Pos_2^j, \ldots, Pos_{Nt}^j\right]$ form trajectory $traj_j$. An example of calculated trajectories is shown in Fig. 6.

D. Step 4: Out of Bounds Trajectories

The trajectories that exceed the area's boundaries, are ignored in the following processes, reducing computational requirements.

E. Step 4: Possible Initial Phase Differences

For antennas' distance greater than $\lambda/2$ the measured phase difference varies within a range greater than 2π, therefore the phase difference is ambiguous. This means that there are

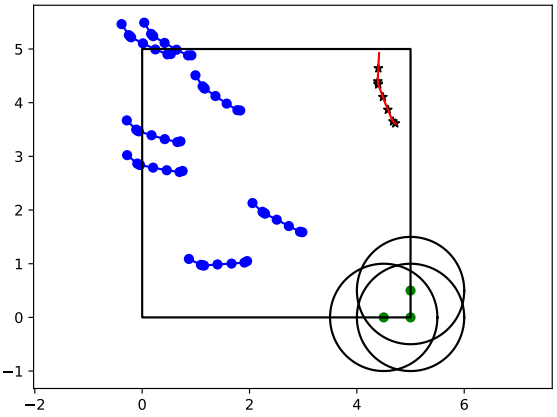

Fig. 6. The three green dots represent the three antennas. The black lines are the boundaries in which the tag can move. The red line is the real trajectory of the tag. The blue lines are possible tag trajectories calculated using phase measurements. Axes unit: m.

multiple branches on which the tag may be, depending on the distance between the antennas.

Let antenna pair $AntPair_{x,y}$ consist of Antenna-x and Antenna-y. The maximum measured phase difference for the pair is:

$$[d\phi_t^{x,y}]_{max} = g(A_x A_y) \quad (33)$$

Let $\phi_{meas}(i,t)$ be the measured phase from Antenna-i at time t, as in (1), and $\phi_{unw}(i,t)$ the same measurements, but unwrapped. The phase difference at t_1 between the antennas of $AntPair_{x,y}$ is calculated:

$$Init^{x,y} = \phi_{unw}(y, t_1) - \phi_{unw}(x, t_1) \quad (34)$$

As stated above, these values are ambiguous. Assuming that the phase measurements are in $[0, 2\pi)$, all the possible phase difference $Real_k^{x,y}$ are $Init^{x,y}$ plus $2k\pi$ offset:

$$Real_k^{x,y} = Init^{x,y} + 2k\pi, \; k \in \mathbb{Z} \quad (35)$$

The values of k are those for which the phase difference values remain measurable:

$$k \in \mathbb{Z} : |Real_k^{x,y}| \leq [d\phi_t^{x,y}]_{max} \quad (36)$$

Let the offsets corresponding to these values of k be:

$$offsets_{x,y} = \left[o_{x,y}|_1, o_{x,y}|_2, \ldots\right] \quad (37)$$

Each offset correspond to a branch, as shown in Fig. 7. Knowing the real phase difference is the same as knowing which must be the offset added to the unwrapped measurements. This offset is constant, since the measurements are unwrapped and explicitly describe how the measured phase changes.

Additionally, each offset in (37) corresponds to a branch-group: Since a branch is defined by an offset, adding that offset to the unwrapped phase difference at another time, and

recalculating the branch with the new phase difference, shows how the branch "moves" with time. Branches of the same offset form a branch-group. An illustration of the "moving" branches is shown in Fig. 8.

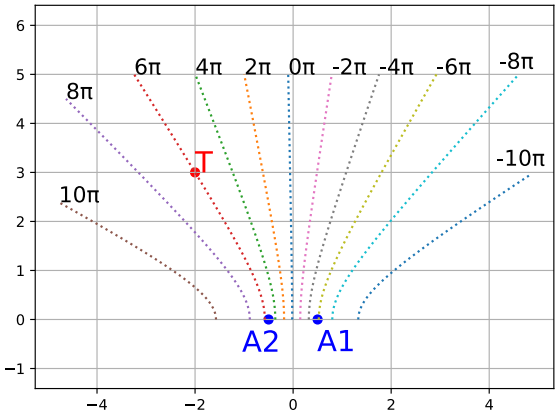

Fig. 7. $A1$ and $A2$ are two antennas interrogating tag T. The dotted lines are the different possible branches on which the tag can be if the measured phase is in $[0, 2\pi)$. The offset added to the measured phase difference is shown for each branch. Axes unit: m.

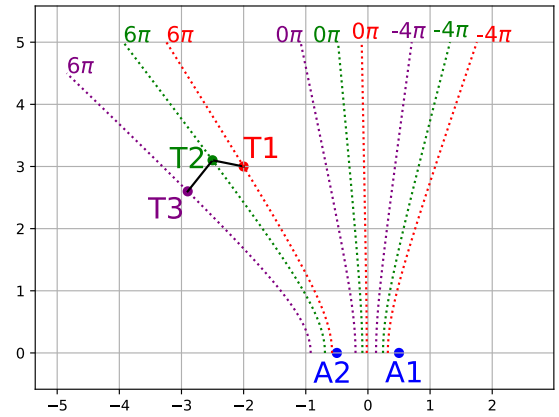

Fig. 8. $A1$ and $A2$ are two antennas interrogating a tag. The tag moves from $T1$ to $T2$ to $T3$ at t_1, t_2, t_3. The dotted lines are some of the different possible branches on which the tag can be if the measured phase is in $[0, 2\pi)$. The offset added to the measured phase difference is shown for each branch. The red branches are those at t_1, the green at t_2, the purple at t_3. Branches calculated using the same offset at different times form a branch-group. They resemble a "moving" branch. Axes unit: m.

F. Step 4: Best Trajectory Calculation

In section II-C1 it was shown that if this phase difference between two antennas is known, the tag should be located on a hyperbola's branch with known equation. Since there are multiple possible phase differences, there are multiple corresponding branches.

The branches calculated by using a constant offset and unwrapped phase measurements at different times, represent the same branch, "moving" as time passes. In other words, if the tag at time t_1 was on branch calculated using an X offset, the branch on which it is at time t_2 must be also calculated using the same X offset.

We compare the possible branches with the possible trajectories to decide which one represents best the real trajectory of the tag. The tag is being interrogated by two antennas, Antenna-1 and Antenna-2.

As shown in section III-E, all the possible offsets for the antenna-pair are calculated:

$$offsets_{1,2} = \left[o_{1,2}|_1 , o_{1,2}|_2 , \ldots \right] \tag{38}$$

For each $traj_j$, at time t_1 , the possible phase differences regarding $AntPair_{1,2}$ are calculated:

$$\left[Init^{1,2} + o_{1,2}|_1 , \; Init^{1,2} + o_{1,2}|_2 , \; \ldots \right] \tag{39}$$

Phase values in (39) are used to calculate branches as shown in section II-C1, and these branches are compared with the trajectory's starting position Pos_1^j.

A_1, A_2 are the positions of Antenna-1 and Antenna-2, and P_{1,t_1}, P_{2,t_1} their projections as in section II-B. We want to determine a branch for each element of (39) as in (24): $d\phi_t^{1,2}$ is a phase difference from (39), and x_0 is calculated using (25):

$$F\left(P_{1,t_1}, P_{2,t_1}, Pos_1^j\right) = \left[x_0, \tilde{Pos}_1^j\right] \tag{40}$$

$\tilde{Pos}_1^j$ is the position of the tag in the new coordinate system. Now the distance between $\tilde{Pos}_1^j$ and the branch can be calculated as in section II-C2. If this is done for every element of (39), we get:

$$\left[dis_{1,2}^j(t_1)\Big|_1 , \;\; dis_{1,2}^j(t_1)\Big|_2 , \;\; \ldots \right] \tag{41}$$

The minimum value of (41) corresponds to the closest branch to Pos_1^j. Only the offset used to calculate this branch is used to calculate branches for the remaining times in $[t_2, t_3, \ldots, t_{Nt}]$. Let that offset be $o_{1,2}^j$:

$$\begin{gathered} o_{1,2}^j = o_{1,2}|_u , \\ \text{where } u = \arg\min_i \left\{ dis_{1,2}^j(t_1)\Big|_i \right\} \end{gathered} \tag{42}$$

The distances between the trajectory's positions and the corresponding branches are calculated. It is recalled that the branches are calculated using the offset $o_{1,2}^j$. The product of these distances is the weight of the trajectory, regarding $AntPair_{1,2}$:

$$w_{1,2}^j = \prod_{k=1}^{Nt} dis_{1,2}^j(t_k)\Big|_u \tag{43}$$

The value of (43) is low, if the branches "follow" the trajectory. The lower the value, the closer the branches are to the trajectory's position.

If the tag is interrogated by multiple antenna-pairs, the same process is repeated for each pair, and the final weight W^j of the trajectory is the product of the weight of each antenna-pair:

$$W^j = \prod w^j_{x,y},\ x, y : \text{all the antenna-pairs} \tag{44}$$

The trajectory with the lowest weight is considered the best representation of the real trajectory of the tag. Simulation results visualizing the weight of the possible trajectories are shown in Fig. 9.

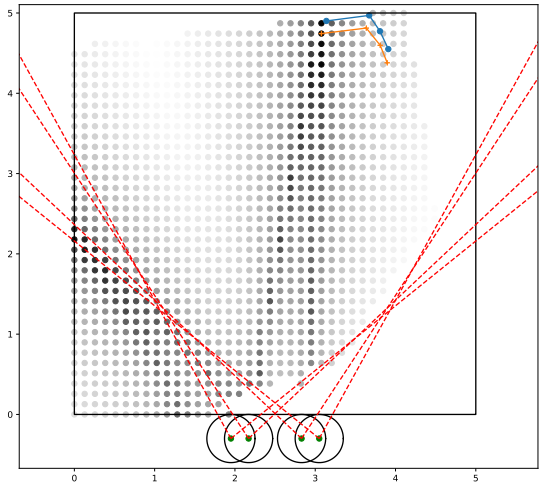

Fig. 9. Simulation results visualizing the weight of the possible positions. The green dots are the positions of the antennas. The black square is the area in which the tag can move. The red dashed lines show the half power beamwidth of each antenna. The dots inside the square are the generated starting positions of the possible trajectories. The darker the color of the dot, the lower its weight: the darkest dot is the starting position of the best trajectory. The orange line is the chosen best trajectory, and the blue line the real one. Axes unit: m.

IV. Simulations

In this section, we examine how the antenna placement and the real trajectory length affect the tracking performance. The results are evaluated based on the mean and median of the $Error$ between the chosen trajectory's positions Pos^j_m and the real positions of the tag at corresponding times:

$$Error = \frac{\sum_{m=1}^{Nt} \left| Pos^j_m - tagTraj(t_m) \right|}{Nt}, \quad j : W^j \text{ is minimum} \tag{45}$$

A. Antenna Placement

Apart from the noise introduced by the reader's electronics, actual measurements suffer from fading, due to multipath. As a result, the estimated trajectories and the hyperbolas created will suffer from errors. Here, we investigate how the locations of the reader's antennas affect the accuracy of the results. The involved antennas should illuminate the same area. Placement of the antennas in close vicinity would facilitate the weighting process (Step 4 of the proposed method), which involves calculating the distance from possible hyperbolas; due to the phase-measurements' ambiguity introduced by the inevitable wrapping of the phase in $[0, 2\pi]$, the number of possible hyperbolas increases as the inter-antenna distance grows. On the other hand, a small inter-antenna distance is expected to increase the error in Step 3, which involves the calculation of the next position, given a known previous position; the reason is that this process involves the cross section of circles centered at each antenna. As the centers of the two circles are nearing, the geometrical dilution of precision increases for the same measurements' error. This is illustrated in Fig. 10. Wrapping up, small inter-antenna distance is expected to facilitate Step 4 but to worsen the accuracy of Step 3 and vice versa.

The above limitations are countered, if more than two antennas are used. If they are placed close to each other in **pairs**, reduced phase-measurement ambiguity is achieved. At the same time, antennas from different pairs have increased inter-antennas distance, and can be used to calculate the possible trajectories.

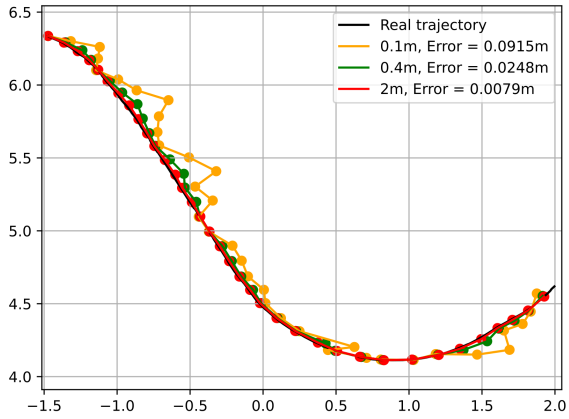

Fig. 10. The $Error$ between the real and the calculated trajectories. Each colored line is the calculated trajectory using antennas with the corresponding inter-antenna distance. As the inter-antenna distance increases, the $Error$ decreases. Axes unit: m.

Different deployment strategies are considered next. The carrier frequency is 867.5 MHz. All antennas are considered at the same height $H_i = 2m$, the tag at $h_t = 1.2m$, so $dh_{i,t} = 0.8m$. The measured phase is calculated using (1), with $s_{phase} = 0.1$. The tag's trajectory $tagTraj(t)$ is randomly generated, starting from a random position, and moving with random sized steps towards a randomly changing direction.

Three or four antennas are used at various formations. Regarding the three-antenna set-ups, the antennas form: 1) a triangle (*triangle*), and 2) a straight line (*line*). In both cases, the antennas are placed as close as possible to each other. As for the four-antenna set-ups, the antennas form: 1) a straight line (*line*), and 2) two pairs on the same line, but at distance from each other (*two pairs*). In these cases, the antennas of each pair are placed as close as possible to each other. The minimum inter-antenna distance is determined by the typical width of reader-antennas. We examine two scenarios, based

on real equipment: 0.20m and 0.125m wide antennas. So, potential inter-antenna distances are 0.22m and 0.15m. The four set-ups mentioned above are implemented with 0.22m inter-antenna distance, and one of them is repeated with 0.15m. So, there are five cases in total. An illustration of the different set-ups is shown in Fig. 11. Details on the set-ups are shown in Table II.

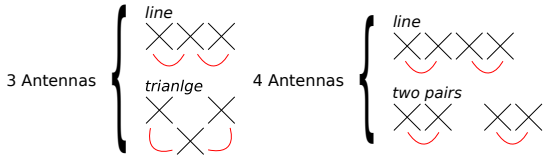

Fig. 11. Illustrations of the different simulation set-ups. In the left half are the three-antenna set-ups, and in the right the four-antenna. The "X" symbols represent the antennas. The red lines show which are the antenna-pairs used to calculate the branches and the weights in each case.

TABLE II
SIMULATION ANTENNA SET-UPS DETAILS.

First Simulation Set				
Set-Up Number	Antennas Number	Antenna Size (m)	Antennas' Positions	Antenna Pairs
#1 (triangle)	3	0.22	$A_1\,(2.344, -0.300)$ $A_2\,(2.500, -0.455)$ $A_3\,(2.655, -0.300)$	A_1, A_2 A_2, A_3
#2 (line)	3	0.22	$A_1\,(2.280, -0.300)$ $A_2\,(2.500, -0.300)$ $A_3\,(2.720, -0.300)$	A_1, A_2 A_2, A_3
#3 (line)	3	0.15	$A_1\,(2.350, -0.300)$ $A_2\,(2.500, -0.300)$ $A_3\,(2.650, -0.300)$	A_1, A_2 A_2, A_3
#4 (line)	4	0.22	$A_1\,(2.170, -0.300)$ $A_2\,(2.390, -0.300)$ $A_3\,(2.610, -0.300)$ $A_4\,(2.830, -0.300)$	A_1, A_2 A_3, A_4
#5 (two pairs)	4	0.22	$A_1\,(1.950, -0.300)$ $A_2\,(2.170, -0.300)$ $A_3\,(2.830, -0.300)$ $A_4\,(3.050, -0.300)$	A_1, A_2 A_3, A_4

In these simulations, the tag can move within the square formed by points $[(0,0),(0,5),(5,5),(5,0)]$. The starting position of the tag can be anywhere in the square. For each antenna-setup we generate the necessary number of random trajectories so that the standard error of the estimated mean given in (45) falls below 3cm. An example of such a trajectory is shown in Fig. 6. The value of $phThr$ is π. In Table III, the mean and median of $Error$ are shown for different values of N_P. In the same Table, the estimation time per position is the total computation time divided by the number of the positions of the calculated trajectory. The results show the following:

- By comparing cases $[\#2, \#3]$, it is shown that different inter-antenna distances of an antenna-pair does not affect the results significantly as long as their difference is small compared to the wavelength. In our case $\lambda/2 \approx 0.17m$, and the inter-antenna distances are $0.22m$ and $0.15m$ ($0.07m$ difference).
- By comparing cases $[\#2, \#4, \#5]$, it is shown that for antenna-pairs on the same axis if the distance between the centers of the pairs is increased, the tracking error is decreased.
- By comparing case #1 to the rest, it is shown that the results are better even though the antenna pairs are close to each other. This case differs to the fact that the antenna-pairs are on different axes. This means that diversity in antenna-pairs' axes is more important than diversity in antenna-pairs' distances.
- In every case, if N_P is increased, the error is decreased.
- Even for the highest value of N_P, the trajectory of the target can be estimated in real-time with less than a 1s delay.

TABLE III
SIMULATIONS: MEAN $Error\ (m)$ / MEDIAN $Error\ (m)$

First Simulation Set			
Set-Up Number	$N_P =$ 500	1000	2000
#1	0.50 / 0.28	0.38 / 0.21	0.33 / 0.16
#2	1.44 / 0.61	1.16 / 0.39	1.04 / 0.31
#3	1.33 / 0.65	1.12 / 0.49	1.02 / 0.41
#4	1.13 / 0.36	0.85 / 0.24	0.60 / 0.18
#5	0.89 / 0.25	0.58 / 0.17	0.38 / 0.11
Est. time	0.22s	0.41s	0.70s

*$phThr = \pi$

It is also worth mentioning that the mean of $Error$ is almost two times greater than the median in every case. High $Error$ values greatly affect the calculated mean. These larger errors arise when the grid of possible starting points is sparse. For $N_P = 500$, the distance between neighboring (possible starting) grid points equals 20cm, whereas for $N_P = 2000$, the corresponding distance is approximately 11.3cm. As a result, in the second case, a possible starting point, generated in the proposed method, may be at most 8cm from the actual position of the tag. As summarized in Table III, many setups address the desired accuracy margin of 1m; however setups #1 and #5 achieve the best performance.

B. Trajectory Length

Here, tag trajectories that resemble a man moving through an exhibition area are examined: in such case, one is expected to move from the entrance to the exit of the area. Such trajectories are simulated assuming that the tag moves in the square formed by points $[(0,0),(0,10),(10,10),(10,0)]$. The entrance is at $(5,0)$, and the tag was first interrogated somewhere close to the door. The exit is somewhere on the upper half of the room. The tag is last interrogated somewhere close to the exit. The three antenna line set-up is used in two cases: 1) the antennas are on $y = -0.3$ centered around $(5,-0.3)$ (*bottom*), and 2) the antennas are on $x = 10.3$ centered around $(10.3,5)$ (*right*). Details on the set-ups are shown in Table IV. In this simulation set, initial positions are only generated near the entrance. A sample of tag trajectories used in these simulations is shown in Fig. 12.

In Table V, the mean and median of $Error$ are shown for different values of N_P. In all cases, the results are satisfying, considering that the trajectory of the tag is easily tracked with a 1-meter error or less, in a 10m x 10m area. It also noted that the results in case #2 are better, because symmetric trajectories

to the axis of symmetry of the antenna set-up (that is $y = 5$) cannot be generated.

TABLE IV
SIMULATION ANTENNA SET-UPS DETAILS.

Second Simulation Set				
Set-Up Number	Antennas Number	Antenna Size (m)	Antennas' Positions	Antenna Pairs
#1 (bottom)	3	0.22	A_1 $(4.78, -0.3)$ A_2 $(5.00, -0.3)$ A_3 $(5.22, -0.3)$	A_1, A_2 A_2, A_3
#2 (right)	3	0.22	A_1 $(10.3, 4.78)$ A_2 $(10.3, 5.00)$ A_3 $(10.3, 5.22)$	A_1, A_2 A_2, A_3

TABLE V
SIMULATIONS: MEAN $Error$ (m) / MEDIAN $Error$ (m)

Second Simulation Set			
Set-Up Number	$N_P =$ 250	500	1000
#1	1.03 / 0.32	0.81 / 0.25	0.62 / 0.20
#2	0.47 / 0.29	0.40 / 0.27	0.36 / 0.27

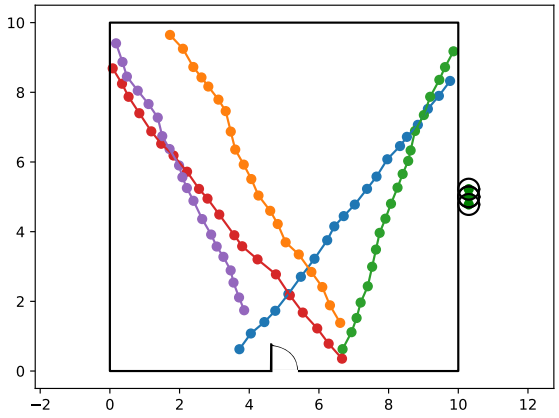

Fig. 12. Sample of tag trajectories used in the second simulation set. The colored lines are different simulated tag trajectories. The black lines are the borders of the simulation area. The green dots on the right are three antennas. The staring positions of the trajectory are close to the "door", shown at the bottom of the square area. Axes unit: m.

V. EXPERIMENTAL RESULTS

Experiments were carried out to verify the simulation results. To collect the phase measurement data an RFID reader (Impinj Speedway R420) was used, operating with four antennas. Specifically, NORDIC ID SAMPO S0 and Laird PER86506 antennas, shown in Fig. 13, were used. They were placed on a banner in a computer lab of the School of Electrical and Computer Engineering of Aristotle University of Thessaloniki.

The target-tag was attached to a robot, as shown in Fig. 13, moving in the computer lab. We used a robot to get the ground truth position of the tag. The robot is equipped with a low-noise 360^o lidar and can perform Simultaneous Localization and Mapping (SLAM) with cm accuracy. Therefore, it creates a map of the environment and calculates its position on that map. The speed of the robot is not constant; it accelerates, decelerates, and even stops as it moves. The map created by the robot, the tag's trajectory, and the positions of the antennas of such an experiment are shown in Fig. 14.

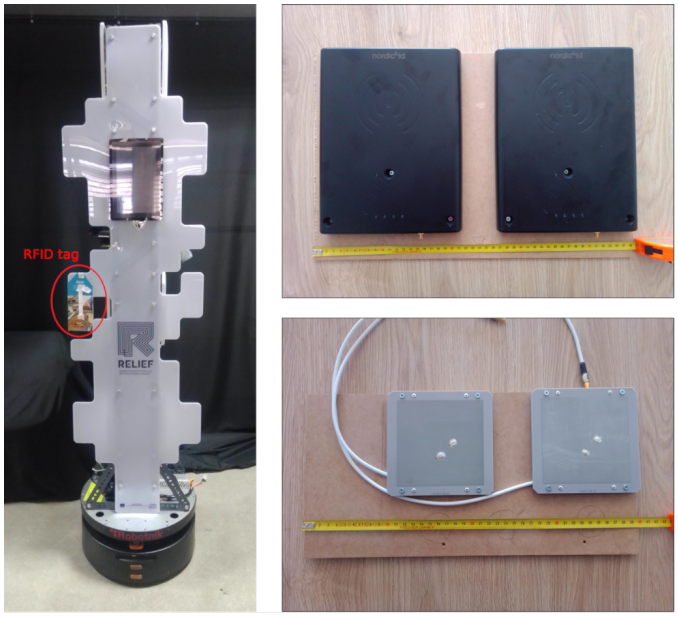

Fig. 13. Left: The robot we used in our experiments. The carried RFID tag can be seen on the left of the picture. Right: The antennas used in our experiments: Top: NORDIC ID SAMPO S0 antennas. Bottom: Laird PER86506 antennas.

Below we examine how the proposed method performs in different cases. We use data from four or three antennas, and assume different areas in which the tag can move, as explained in section III-D: a "bounded" and an "unbounded" area are examined. The first is the part of the room that the antennas can see, based on their radiation pattern, and the latter the perimeter of the room without considering any obstacles in it. Additionally, different values of $phThr$, introduced in section III-B, are tested. Finally, the experiments are evaluated with respect to the achieved $Error$, shown in (45). From each case different conclusions are drawn.

A. Case A: Experiment #1, Four Antennas, "Bounded" Area

The set-up of this case is that of Fig. 14. Data from four antennas are used. The two antenna-pairs used to apply the proposed method are the two antennas on the left, and the two antennas on the right (Fig. 14). The estimated trajectory is shown in Fig. 15. The trajectory appears "spiky" due to the noise of the measurements.

It is reminded that the time-set used in calculations and the starting positions are randomly generated, as explained in sections III-B and III-C. This means that different runs of the algorithms produce different results. To decide which is the trajectory of the tag, we average the results of N_A different runs. The mean $Error$ for an increasing N_A, but for the same

N_P is shown in Table VI. As N_A increases, the error decreases and "converges" to a value which is limited by the noise of the measurement data. We want to clarify that, for different runs of the algorithms, the randomly chosen data used for the calculations are differently affected by the noise: in some cases the error was close to 1m, in others less than 10cm. The minimum error we recorded being calculated was 4.31cm. But, in the proposed, there is not a way to know in advance which measurement data is "good" or "bad", so our averaging approach is utilized.

TABLE VI
EXPERIMENT RESULTS,
INCREASING N_A FOR CONSTANT N_P.

Case A				
$N_P =$ $N_A =$	100 1	100 5	100 10	100 20
Mean $Error(m)$	0.33	0.18	0.15	0.13
$N_P =$ $N_A =$	200 1	200 5	200 10	200 20
Mean $Error(m)$	0.28	0.15	0.13	0.12

*$phThresh = \pi$

We also examine the effect of the number of the generated starting positions N_P. In Table VII the mean $Error$ for different values of N_P is shown, while the product $N_A \times N_P$ remains constant, thus maintaining the running-time nearly constant. As N_A increases, the error is reduced. In Table VIII, the mean $Error$ for different value of $phThresh$ is shown. The $Error$ is the same for all cases. It is reminded that lower $phThresh$ values mean more elements in each time-set, thus more computational requirements, but a more detailed calculated trajectory.

TABLE VII
EXPERIMENT RESULTS,
CONSTANT $N_A N_P$ PRODUCT.

Case A				
$N_P =$ $N_A =$	1000 1	500 2	200 5	100 10
Mean $Error(m)$	0.23	0.20	0.17	0.15
$N_P =$ $N_A =$	2000 1	400 5	200 10	100 20
Mean $Error(m)$	0.21	0.16	0.13	0.13

*$phThresh = \pi$

TABLE VIII
EXPERIMENT RESULTS,
$phThresh$ VARIATION.

Case A				
$phThresh =$	2π	π	$\pi/2$	$\pi/4$
Mean $Error(m)$	0.13	0.13	0.12	0.13

*$N_P = 100,\ N_A = 10$

B. Case B: Experiment #1, Four Antennas, "Unbounded" Area

In this case, the same data as in section V-A are used. But now the simulated area in which the tag can move is larger:

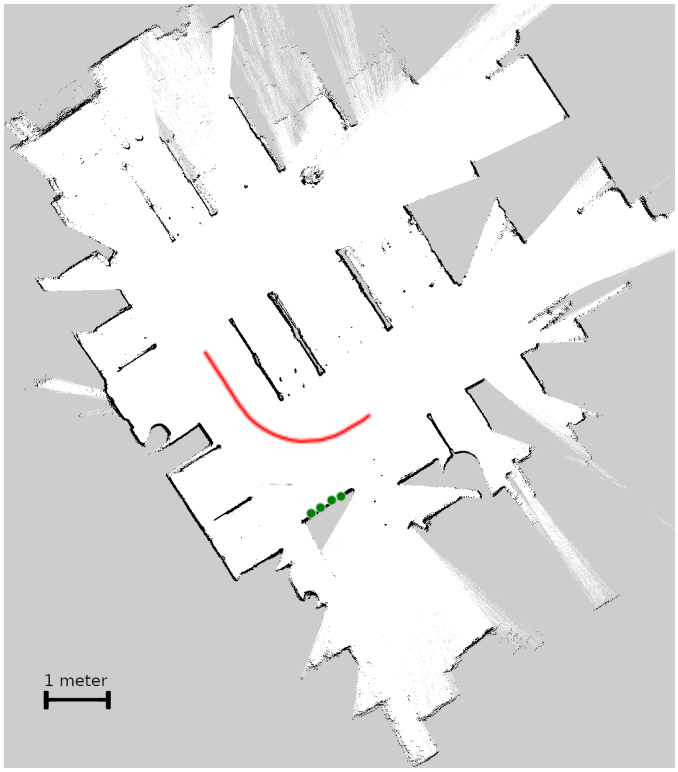

Fig. 14. The map of the experiment area created by the robot. The red line shows the trajectory of the robot carrying the tag. The green dots show the position of the four antennas.

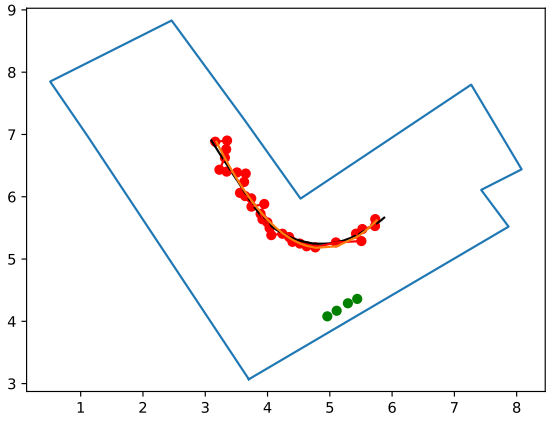

Fig. 15. The results of a run of the algorithm. The blue line shows the borders of the area in which the tag can move. The green dots are the positions of the antennas. The black line is the trajectory of the tag. The red line is the calculated trajectory of the tag. The orange line is a smoothed approximation of the calculated trajectory. Axes unit: m.

the antennas are placed in the middle of a side of a 10m x 10m square. Compared with case A, the simulated area is five times larger, and without any obstacles in it. This means that the generated starting positions are sparser. In Table IX, the results for constant $N_P N_A$ are shown. In contrary with the results of Table VII, higher N_A values do not result to lower error. Low N_P values means that it is more likely that staring positions are not generated close enough to the real one. So, the error in such a case will be high. As a rule of thumb, the distance between neighboring grid points should not exceed 45cm.

TABLE IX
EXPERIMENT RESULTS, CONSTANT $N_A N_P$ PRODUCT.

Case B			
$N_P =$	1000	500	100
$N_A =$	1	2	10
Mean $Error(m)$	0.30	0.30	0.88

*$phThresh = \pi$

C. Case C: Experiment #1, Three Antennas, "Bounded" Area

In this case, the same data as in section V-A are used, but the phase measurement from only three antennas are utilized. The three rightmost antennas of Fig. 14 are used. The mean $Error$ for $N_P = 100$, $N_A = 10$, and $phThresh = \pi$ is 0.34m. Compared to the four-antenna case, the error is slightly higher. This is a very important property, since data may not be available from all four antennas in practical applications.

D. Case D: Experiment #2, Four Antennas, "Bounded" Area

In this case, a different antenna set-up was used. The trajectories of the robot, the created map, and the position of the antennas are shown in Fig. 16. Three robot trajectories were tested. In all cases, the proposed method accurately calculated the trajectory of the tag, achieving errors below 0.5m. Specifically, the calculated errors for $N_P = 100$, $N_A = 10$, and $phThresh = \pi$, are 0.34m for #1, 0.47m for #2, and 0.42m for #3.

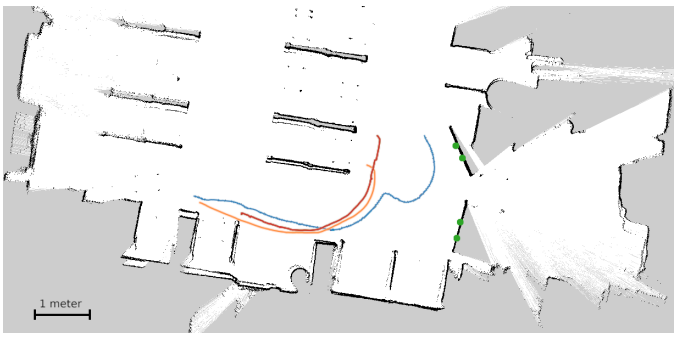

Fig. 16. The map of the experiment area created by the robot. The blue (#1), orange (#2), and red (#3) lines show the trajectories of the robot carrying the tag. The green dots show the position of the four antennas.

E. Extension of the method in 3D space

In the analysis so far, we have assumed that the height of the tag is fixed (and known). Such assumption is valid for most practical applications, since indoor movements are typically carried out along a specific plane. However, the actual height of the tag may not be known. To tackle this problem, one should initially divide 3D space in different planes parallel to the ground. Then the method is applied along each plane; i.e. assuming that the tag lies on the specific plane. Finally, the trace that minimizes the cost function among all traces along different planes is selected. The only drawback is that the estimation-time will be multiplied with the number of planes.

Such a result is presented next. We repeat Experiment #1 in section V-A for two additional possible planes: 1) assuming the tag moves 0.25cm below the actual path and 2) assuming the tag moves 0.25cm above the actual plane. The best trajectory for each of the three planes is shown in Fig. 17. The following conclusions are drawn:

- The best trajectory overall (that minimizes the cost function) is the one on the actual height of the tag.
- The trajectory with +0.25cm erroneous height-displacement is shifted away (with respect to the antennas) from the actual trajectory.
- The trajectory with -0.25cm erroneous height-displacement is shifted closer (with respect to the antennas) from the actual trajectory.
- In both cases the resulted trajectory is very close to the actual trajectory; i.e. the error is small.

It is reminded that our practical problem is to track visitors roaming inside an archaeological museum. The ticket is fastened on one's arm. Therefore, the variability of the expected height depends mainly on the height of the visitor and will not exceed 50cm. Thus, the proposed method will deliver accurate results even if the estimations are carried out only for the average expected height.

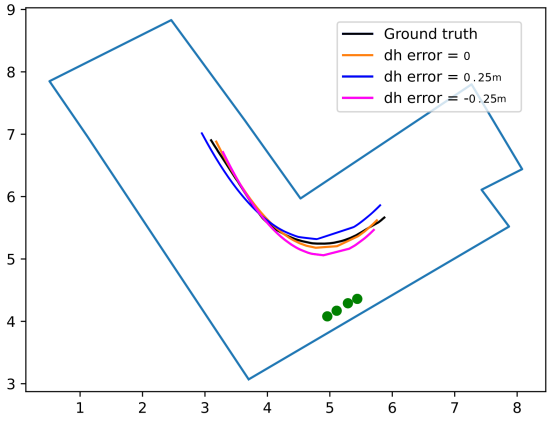

Fig. 17. The resulted trajectories for different assumed height difference between the antennas and the tag. The ground truth is the black line. The real height is dh, and the corresponding calculated trajectory is the orange one. The blue and pink lines are the resulted trajectories if the height difference is assumed $dh + 0.25m$ and $dh - 0.25m$ correspondingly. Axes unit: m.

VI. Comparison with Prior Art

In this section, we compare the proposed method with prior art. The same data from the experiments described in section V are used. The only method that shares the same assumptions is Tagoram from [15]. Those common constraints are: both methods track a single moving RFID tag using POA measurements from multiple antennas, utilizing one carrier frequency, the trajectory is arbitrary and the initial position is unknown.

In Tagoram, antennas at known locations receive phase measurement from a moving tag. The initial position of the tag is assumed on a grid on the monitored area. For each grid position, utilizing consecutive phase measurements differences, the velocity of the target is estimated, using radial velocity vectors. Instead of the target, the antennas are "virtually" moved with the opposite velocity. Then, the measured phase differences from the antennas are compared to the theoretical values. Weights are assigned to the grid positions. The grid position with the highest weight is considered the initial position of the target, and its trajectory is calculated in the same manner as above

The data from experiments of sections V-A and V-D are used. For both methods, the grid size as well as the number of positions of the resulting trajectory are equal. The pre-processing of the phase measurement data is the same. Table X shows the results of the proposed method and of Tagoram, as well as the corresponding computation times (C.T.). The proposed method is more accurate than Tagoram in all experiments. More importantly, the computation time of the proposed method outperforms Tagoram significantly.

We believe that the use of *radial velocity vectors*, often used in literature to calculate the velocity of moving targets, is only effective when the monitoring antennas are spatially distributed in a way that the radial vectors to the target are perpendicular to each other. Only then can the target's velocity be accurately described. In our experiments, few positions of the real trajectory meet that condition. Additionally, in Tagoram, a minimization problem is solved for the calculation of the real velocity at every position. Thus, the computational requirements are increased.

TABLE X
Method Comparison.

Proposed Method, $N_P = 100, N_A = 10$				
Experiment	V-A	V-D #1	V-D #2	V-D #3
$Error(m)$	0.15	0.34	0.47	0.42
$C.T.(s)$	~ 10	~ 17	~ 19	~ 11

Tagoram, $GridSize = 1000$				
Experiment	V-A	V-D #1	V-D #2	V-D #3
$Error(m)$	1.27	3.74	0.70	1.32
$C.T.(s)$	~ 615	~ 1109	~ 759	~ 746

*$C.T. = Computation\ Time$

VII. Limitations and Future Work

We have put forward a prototype approach to track moving RFID tags from a set of antennas fixed at known positions. Applicability of the method is constrained on the motion of the target and the tracked population; the number of tracked tags within the range of the antennas. If the target is stationary, it cannot be tracked, since the antennas would measure a constant phase. The method exploits the variation of the phase, as measured from different known locations.

The method requires phase-unwrapping. Phase unwrapping depends on the target-tags' population, the reader's read-rate, the number of antennas and each target-tag's velocity. Let R reads/s be the reader's read-rate, M the number of antennas connected to the same reader, N the number of tags and V the magnitude of the tag's velocity. Let a tag move radially from/to a reader's antenna. The measured phase of the tag would change by 2π every $\lambda/2$ of displacement. This would take place every $\Delta t = \frac{\lambda}{2}V$. Considering that we need at least two samples per 2π to perform phase unwrapping, the minimum necessary read-rate per tag is $r_{min} = 2/\Delta t$ reads/s. Assuming an even distribution of the available timeslots of a reader to its connected antennas and to the tags' population, each tag will be measured at a rate $r = \frac{R}{MN}$. From the above, it follows that r should be greater than r_{min}. Furthermore, the maximum population of tags that can be tracked concurrently are:

$$N_{max} = \frac{R}{Mr_{min}} = \frac{R\Delta t}{2M} = \frac{R\lambda}{4VM} \tag{46}$$

Let's consider the typical values of the variables in the above equation, assuming the EPC UHF Gen2 Air interface protocol. The reader transmits successively through 4 antennas. It is expected to read at $R = 200$ reads/s. The average walking speed is 1.4m/s; a person at an exhibition is expected to move at half the above speed, i.e. 0.7m/s. The wavelength is approximately 34cm. By substituting, the system may track concurrently up to 6 visitors. Considering passive RFID tags, the maximum expected range of UHF RFID equipment is approximately 10m. The number of people moving in such an exhibition area is limited. As the visitors move, they will be identified by subsequent readers/antennas every 10m of displacement. However, it is expected that there will be cases that suitable measurement conditions will not be met: either the read rate will be too low, or the target tag will be blocked, e.g. by the human body.

In an effort to improve the number of tracked tags, one might argue to increase the number of readers with overlapping coverage areas. However, due to the protocol, a tag associated with a reader would not respond to the interrogation of the second reader in the following time-slots, as required by the method. Another alternative to increase the number of tracked tags is to exploit only two reader antennas, which is the minimum number of antennas required by the method. Again, this is not a good practice, due to multipath fading. Destructive summation of multipath contributions results in minimums of the field inside the area. Consequently, there are parts of the motion of the tag that are measured by a subset of the available antennas; so a better strategy is to keep 4 antennas active, in order to make sure that at least two antennas measure the target throughout its motion.

To improve performance, future work can be focused on the better utilization of the collected phase measurements. For

example, dividing the measurements to intervals that can be unwrapped. And in the same manner, to intervals depending on which antennas can see the target. Using these information, phase measurement subsets suitable for applying the proposed method can be created. Then, by fusing the results of each measurement subset, the total trajectory of the target will be estimated.

Attachment of the tag to the visitor sets new challenges that need to be met. The tag's antenna must be suitably decoupled from the adjacent human body; it should either include a ground plane, or be fixed away from one's body, by properly introducing a distancer between the body and the tag. The tag will be attached on the arm or on the shoulder by means of an armband or it will be hung from the neck inside a card-holder. The distancer will be fixed inside the armband or the card holder. Depending on the location of the tag with respect to the body and the installed equipment, there will be areas, where the body might block the reader-to-tag link. From such perspective the visitor's shoulder represents the best pick for placement of the tag, but also the most annoying location for the visitor. Local motion of the visitor's body is also expected to affect the method; for example, if the tag is attached on the arm, the visitor is expected to move the arm back and forth while walking. This motion is expected to look like the "noise" in the measurements and will be smoothed by the applied filter. The tag's antenna is not expected to operate in proximity with other tags.

Multipath is not expected to significantly affect the accuracy of tracking, as was experienced by the measurements with the robot, which were conducted in a "multipath-rich" indoor office environment. The main reason behind this advantageous property is the necessity of a strong Line-Of-Sight component for the battery-less RFID technology to operate. The presence of the direct path dominates the multi-ray power profile of the link. The reader measures the phase of the resultant field from all contributions (including possible strong reflections and scattering), but all other rays are expected to be significantly smaller than the direct path and hence the variation of the measured phase from the expected phase of the direct path is expected to be small.

However, multipath is expected to strongly affect the performance of the method if the range of the installation increases. This could take place either by selecting active RFID tags or by installing RFID repeaters [28], [29]. Under such conditions, the method needs to be evaluated again.

VIII. Conclusions

In this paper, we have presented a prototype RFID trajectory tracking method. It exploits phase measurements from multiple antennas (at least two are required), calculates possible tag trajectories, without knowledge of the initial position of the target, and assigns weights to them to find the best representation of the actual trajectory. The computational requirements are low enough to enable real-time applications. Both the trajectory tracking accuracy and the estimation-time are greatly improved compared to prior art.

Experimental results, presented in Tables VI and VII validate an expected trade-off between accuracy and running-time. It is shown that we can achieve a mean error of 30cm for estimation-time as low as 40ms. The error falls below 20cm if we allow 200ms running-time and can be further reduced below 15cm, depending on the density of the calculations' grid. In all cases, the accuracy is exceptional for any typical application.

Future work will be focused on the extension of the method for longer ranges, which may suffer from increased multipath fading, decoupling of the tag from the human body and experimental investigation of the effects of larger tagged populations moving around the same area.

References

[1] Kang-Kang Duan, Shuang-Yin Cao, "Emerging RFID technology in structural engineering – A review," Structures, Volume 28, 2020, Pages 2404-2414, ISSN 2352-0124, https://doi.org/10.1016/j.istruc.2020.10.036.

[2] J. Zhang, G. Tian, A. Marindra, A. Sunny, and A. Zhao, "A Review of Passive RFID Tag Antenna-Based Sensors and Systems for Structural Health Monitoring Applications," Sensors, vol. 17, no. 2, p. 265, Jan. 2017.

[3] H. Wang and W. Gong, "RF-Pen: Practical Real-Time RFID Tracking in the Air," in IEEE Transactions on Mobile Computing, doi: 10.1109/TMC.2020.2997080.

[4] Jue Wang, Deepak Vasisht, and Dina Katabi. 2014. RF-IDraw: virtual touch screen in the air using RF signals. SIGCOMM Comput. Commun. Rev. 44, 4 (October 2014), 235–246. DOI:https://doi.org/10.1145/2740070.2626330

[5] Longfei Shangguan, Zimu Zhou, and Kyle Jamieson. 2017. Enabling Gesture-based Interactions with Objects. In Proceedings of the 15th Annual International Conference on Mobile Systems, Applications, and Services (MobiSys '17). Association for Computing Machinery, New York, NY, USA, 239–251. DOI:https://doi.org/10.1145/3081333.3081364

[6] X. Lu, L. Wang, D. Zhao and C. Zhai, "Multi-tag RFID System Enables Localization and Tracking," Journal of Physics: Conference Series. 1168. 022103, 2019, doi: 10.1088/1742-6596/1168/2/022103.

[7] C. Wang, L. Xie, K. Zhang, W. Wang, Y. Bu and S. Lu, "Spin-Antenna: 3D Motion Tracking for Tag Array Labeled Objects via Spinning Antenna," IEEE INFOCOM 2019 - IEEE Conference on Computer Communications, Paris, France, 2019, pp. 1-9, doi: 10.1109/INFOCOM.2019.8737372.

[8] T. Kanda, M. Shiomi, L. Perrin, T. Nomura, H. Ishiguro and N. Hagita, "Analysis of People Trajectories with Ubiquitous Sensors in a Science Museum," Proceedings 2007 IEEE International Conference on Robotics and Automation, Roma, 2007, pp. 4846-4853, doi: 10.1109/ROBOT.2007.364226.

[9] Mugahid Omer, Gui Yun Tian, "Indoor distance estimation for passive UHF RFID tag based on RSSI and RCS," Measurement, Volume 127, 2018, Pages 425-430, ISSN 0263-2241, https://doi.org/10.1016/j.measurement.2018.05.116.

[10] M. Scherhäufl, M. Pichler, E. Schimbäck, D. J. Müller, A. Ziroff and A. Stelzer, "Indoor Localization of Passive UHF RFID Tags Based on Phase-of-Arrival Evaluation," in IEEE Transactions on Microwave Theory and Techniques, vol. 61, no. 12, pp. 4724-4729, Dec. 2013, doi: 10.1109/TMTT.2013.2287183.

[11] S. Sarkka, V. V. Viikari, M. Huusko and K. Jaakkola, "Phase-Based UHF RFID Tracking With Nonlinear Kalman Filtering and Smoothing," in IEEE Sensors Journal, vol. 12, no. 5, pp. 904-910, May 2012, doi: 10.1109/JSEN.2011.2164062.

[12] Y. Zhang, M. Amin and K. Shashank, "Localization and Tracking of Passive RFID Tags Based on Direction Estimation," International Journal of Antennas and Propagation, 2007, doi: 10.1155/2007/17426.

[13] A. Parr, R. Miesen and M. Vossiek, "Inverse SAR approach for localization of moving RFID tags," 2013 IEEE International Conference on RFID (RFID), Penang, 2013, pp. 104-109, doi: 10.1109/RFID.2013.6548142.

[14] C. Jiang, Y. He, X. Zheng and Y. Liu, "Orientation-Aware RFID Tracking with Centimeter-Level Accuracy," 2018 17th ACM/IEEE International Conference on Information Processing in Sensor Networks (IPSN), Porto, 2018, pp. 290-301, doi: 10.1109/IPSN.2018.00057.

[15] L. Yang, Y. Chen, X. Li, C. Xiao and Y. Liu, "Tagoram: Real-time tracking of mobile RFID tags to high precision using COTS devices," Proceedings of the Annual International Conference on Mobile Computing and Networking, MOBICOM, 2014, doi: 10.1145/2639108.2639111.

[16] Z. Chen, P. Yang, J. Xiong, Y. Feng and X. -Y. Li, "TagRay: Contactless Sensing and Tracking of Mobile Objects using COTS RFID Devices," IEEE INFOCOM 2020 - IEEE Conference on Computer Communications, Toronto, ON, Canada, 2020, pp. 307-316, doi: 10.1109/INFOCOM41043.2020.9155531.

[17] J. Wang, J. Xiong, H. Jiang, X. Chen and D. Fang, "D-Watch: Embracing "Bad" Multipaths for Device-Free Localization With COTS RFID Devices," in IEEE/ACM Transactions on Networking, vol. 25, no. 6, pp. 3559-3572, Dec. 2017, doi: 10.1109/TNET.2017.2747583.

[18] Lei Yang, Qiongzheng Lin, Xiangyang Li, Tianci Liu, and Yunhao Liu. 2015. See Through Walls with COTS RFID System! In Proceedings of the 21st Annual International Conference on Mobile Computing and Networking (MobiCom '15). Association for Computing Machinery, New York, NY, USA, 487–499. DOI:https://doi.org/10.1145/2789168.2790100

[19] D. Zhang, J. Ma, Q. Chen and L. M. Ni, "An RF-Based System for Tracking Transceiver-Free Objects," Fifth Annual IEEE International Conference on Pervasive Computing and Communications (PerCom'07), White Plains, NY, 2007, pp. 135-144, doi: 10.1109/PERCOM.2007.8.

[20] D. Zhang et al., "Fine-Grained Localization for Multiple Transceiver-Free Objects by using RF-Based Technologies," in IEEE Transactions on Parallel and Distributed Systems, vol. 25, no. 6, pp. 1464-1475, June 2014, doi: 10.1109/TPDS.2013.243.

[21] P. Bahl and V. N. Padmanabhan, "RADAR: an in-building RF-based user location and tracking system," Proceedings IEEE INFOCOM 2000. Conference on Computer Communications. Nineteenth Annual Joint Conference of the IEEE Computer and Communications Societies (Cat. No.00CH37064), Tel Aviv, Israel, 2000, pp. 775-784 vol.2, doi: 10.1109/INFCOM.2000.832252.

[22] K. Wu, Jiang Xiao, Youwen Yi, Min Gao and L. M. Ni, "FILA: Fine-grained indoor localization," 2012 Proceedings IEEE INFOCOM, Orlando, FL, 2012, pp. 2210-2218, doi: 10.1109/INFCOM.2012.6195606.

[23] M. Ciurana, F. Barcelo-Arroyo and S. Cugno, "A novel TOA-based indoor tracking system over IEEE 802.11 networks," 2007 16th IST Mobile and Wireless Communications Summit, Budapest, 2007, pp. 1-5, doi: 10.1109/ISTMWC.2007.4299293.

[24] R. Zhou, M. Tang, Z. Gong and M. Hao, "FreeTrack: Device-Free Human Tracking With Deep Neural Networks and Particle Filtering," in IEEE Systems Journal, vol. 14, no. 2, pp. 2990-3000, June 2020, doi: 10.1109/JSYST.2019.2921554.

[25] J. Luo, C. Zhang and C. Wang, "Indoor Multi-Floor 3D Target Tracking Based on the Multi-Sensor Fusion," in IEEE Access, vol. 8, pp. 36836-36846, 2020, doi: 10.1109/ACCESS.2020.2972962.

[26] J. Shackleton, B. VanVoorst and J. Hesch, "Tracking People with a 360-Degree Lidar," 2010 7th IEEE International Conference on Advanced Video and Signal Based Surveillance, Boston, MA, 2010, pp. 420-426, doi: 10.1109/AVSS.2010.52.

[27] J. Ong, B. -T. Vo, B. -N. Vo, D. Y. Kim and S. Nordholm, "A Bayesian Filter for Multi-view 3D Multi-object Tracking with Occlusion Handling," in IEEE Transactions on Pattern Analysis and Machine Intelligence, doi: 10.1109/TPAMI.2020.3034435.

[28] S. Megalou, A. G. Dimitriou, A. Tzitzis and T. V. Yioultsis, "Design and Fabrication of a Compact, Low-Cost UHF-RFID Repeater, Exploiting Circular Cross-Polarization," in IEEE Journal of Radio Frequency Identification, doi: 10.1109/JRFID.2020.3040439.

[29] A. G. Dimitriou, "Design, Analysis, and Performance Evaluation of a UHF RFID Forward-Link Repeater," in IEEE Journal of Radio Frequency Identification, vol. 4, no. 2, pp. 73-82, June 2020, doi: 10.1109/JRFID.2019.2953785.

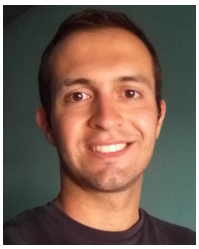

Aristidis Raptopoulos Chatzistefanou was born in Florina, Greece, in 1996. He received the Diploma degree in electrical and computer engineering from the Aristotle University of Thessaloniki in 2019, where he is currently pursuing the Ph.D. degree, and working as a Research Assistant with the Aristotle University of Thessaloniki. His main research interests include RFID technology, localization and tracking techniques.

Anastasios Tzitzis was born in Thessaloniki, Greece, in 1994. In 2018 he received the Diploma in Electrical and Computer Engineering from Aristotle University of Thessaloniki, where he is currently working toward the Ph.D. degree. At the same time, he is working as a Research and Teaching Assistant at the Aristotle University. His current research interests include analysis and design of antennas, RFID technology and wave propagation.

Spyros Megalou received the MSc degree in Electrical and Computer engineering from the Aristotle University of Thessaloniki, Greece, in 2019, and he is currently pursuing the Ph.D. degree at the same School. His main research interests include RFID technology, localization techniques, microwave applications and antenna design. He is also a member of a space related group (BEAM, Beyond Earth Aristotle Missions) focusing on space experiments and applications.

George Sergiadis received his diploma in Electrical Engineering from the Aristotle University of Thessaloniki, Greece, and his Ph.D. from "Ecole Nationale Supérieure des Télécommunications", in Paris, France.

He is currently full Professor at the Aristotle University of Thessaloniki, Greece, teaching Telecommunications and Biomedical Engineering, since 1985. He has been an August-Wilhelm Scheer visiting professor in TUM, Munich, Germany, a visiting researcher at Media Lab, MIT, also in IBMI, Munich, Germany, and a Distinguished Professor at SIBET, Suzhou, China, for several years.

His current research interests include signal and image processing, and medical imaging.

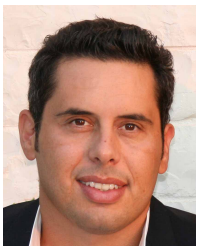

Antonis G. Dimitriou (S'01-M06-SM'14) received the diploma and the Ph.D. degree in Electrical and Computer Engineering from the Aristotle University of Thessaloniki, Greece, in 2001, and 2006 respectively. Since 2007, he is with the School of Electrical and Computer Engineering of AUTh, where he currently serves as a teaching and research faculty member.

He has participated in more than 20 research projects, 8 of which since 2007 as a principal investigator in the fields of Robotics, RFIDs, and Wireless Sensor Networks. He is currently the coordinator of project "RELIEF", involving continuous RFID inventorying through robotics and project "CULTUREID", where RFID equipment will be installed inside the Archaeological Museum of Thessaloniki to monitor RFID tagged exhibits and track visitors. He was a Management Committee Member in the ICT COST Action IC301 "Wireless Power Transmission for Sustainable Electronics (WiPE)". He is the author or co-author of approximately 60 journal and conference papers.

Dr. Dimitriou was the recipient of the Ericsson Award of Excellence in Telecommunications in 2001 and co-recipient of the student-paper award in the 2011 IEEE RFID-TA conference. He received the "IEEE Wireless Communications Letters Exemplary Reviewer" award in 2012 and 2014. He is a Senior IEEE Member since February 2014. He also serves as a reviewer for major journals and as a TPC member for international conferences.